Challenges in the Design of a 100 kW Induction Motor for a PHEV Application

J. Herbst, J. Hahne, H. Jordan, H. Liu, A.Gattozzi
University of Texas Center for Electromechanics
Austin, Texas
www.utexas.edu/research/cem/

Ben Wu
TECO-Westinghouse Motor Company
Round Rock, Texas
www.tecowestinghouse.com

***Abstract*—This paper summarizes some design challenges encountered in the development of a high speed induction motor/generator for a plug-in hybrid electric vehicle (PHEV). The traction system motor/generator was developed for integration into a high performance full-sized passenger car being developed by a major automotive manufacturer. The paper summarizes the traction motor performance requirements and presents the electromagnetic, mechanical and thermal design issues of the high speed 100 kW peak power induction machine.**

Keywords—Plug-in hybrid electric vehicle, PHEV, high speed induction motor, high speed induction generator

I. INTRODUCTION

The University of Texas at Austin Center for Electromechanics (UT-CEM) and TECO-Westinghouse Motor Company (TWMC) teamed to develop designs for a high speed induction motor/generator and associated motor drive for a plug-in hybrid electric vehicle (PHEV). The traction motor/generator and motor controller designs were developed in support of a full-sized, PHEV passenger car being developed by a major international automotive manufacturer. The short schedule for the motor development program imposed constraints on the manufacturing and assembly techniques considered for the prototype machine.

Integration of the induction motor/generator and motor control system into the PHEV chassis limited the size, weight, and configuration of the propulsion system component designs. The vehicle driveline configuration and performance specifications dictated the performance requirements for the traction system components.

II. PERFORMANCE/INTEGRATION REQUIREMENTS

Vehicle integration issues dictated the traction motor envelope dimensions and the location of mounting tabs and electrical terminals. The totally enclosed, liquid cooled traction motor was designed to mount directly to the case of the single-speed vehicle transmission and this interface defined the shaft, front flange and bolt pattern for the traction motor. Performance curves and efficiency maps covering the design speed and power range were also included in the design specification. Additional detail on the performance requirements is presented in the section on electromagnetic design. Table I summarizes some of the key traction system parameters considered in the design of the induction motor/generator.

TABLE I. TRACTION MOTOR PERFORMANCE REQUIREMENTS

Parameter	Specification
Motor Type	Induction
Cooling	Liquid
Operating Speed	0 – 9,600 rpm
Maximum Power	100 kW for 30 s
Continuous Power	> 50 kW
Starting Torque	234 Nm @ < 500 rpm for 10 s
Efficiency	> 90%
Nominal Battery Voltage	326 Vdc
Maximum Battery Voltage	377 Vdc
Minimum Battery Voltage	255 Vdc
Target Weight – Motor	< 70 kg
Maximum Length	370 mm
Maximum Diameter	270 mm

In addition to the physical constraints and performance requirements, the design specification also defined the ambient temperature, coolant inlet temperature, coolant flowrate, and allowable temperature rise for the liquid cooling system. Vehicle integration constraints on the power converter and the characteristics of the battery system limited the current capacity of the variable frequency drive to approximately 800. Although the inverter design issues are not presented in this paper, this design constraint was a driving factor in the design of the traction motor.

III. ELECTROMAGNETIC DESIGN

The motor performance specifications were quite demanding, as is the case for many traction motors. The application required high volumetric and gravimetric power density and the torque demands were quite high, particularly at low speed. Rapid acceleration and hill climbing capability dictated these high torque requirements.

Additional aspects of the motor specifications at various speeds and load conditions are presented in Table II. To enable development of the baseline design, the motor was nominally rated at 50 kW, 5,000 rpm, and 200 Vac. For the 4-pole design, this corresponds to a base frequency of 167 Hz.

Although not specified in Table II, there was a requirement that the motor efficiency at both 50 and 100 kW and 5,000 rpm must exceed 90%. This efficiency requirement and the torque requirements in the 0 to 3,000 rpm speed range proved to be the pivotal specifications and, therefore, the focus of most of

the design effort. Figure 1 summarizes the motor power and torque over the operating speed range from 500 to 9,600 rpm.

The following sections provide more details of the motor specifications and the design developed to meet the specifications.

TABLE II. TRACTION MOTOR SPECIFICATIONS

Parameter	Specification
Maximum Power/Torque 30 s Rating	100 kW @ 4,800 – 6,000 rpm 260 Nm @ 3,000 rpm
Intermediate Power/Torque 3 min. Rating	80 kW / 208 Nm
Intermediate Torque 10 s Rating	234 Nm @ 500 rpm
Nominal Power/Torque Continuous Rating	50 kW @ 4,800 – 9,600 rpm[1]
Regeneration Mode 30s Rating	50 kW @ 4,800 – 9,600 rpm[1]

1. See performance curves

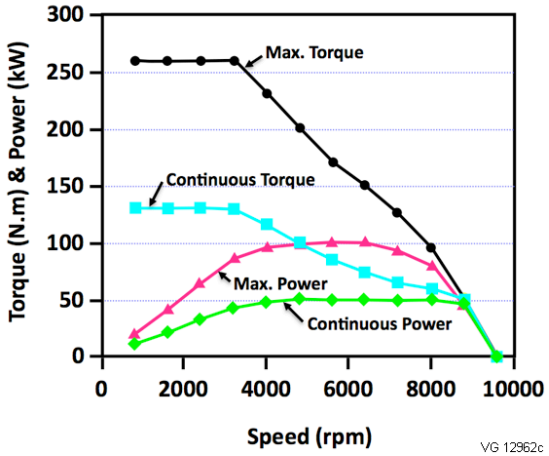

Figure 1. Traction motor design performance curves

A. *Traction Motor Design*

An algorithm based design code, VICA, was used to explore the design space for the induction machine prior to performing more detailed finite element analysis of the machine. The baseline motor design featured 48 stator slots and 38 rotor bars. The armature winding was a 4-pole random wound configuration and the rotor was a conventional squirrel cage design. Due to the schedule constraints, fabricated copper bar construction was planned for the prototype; cast aluminum construction was considered for the production machines.

Meeting the torque specifications, particularly in the starting and low-speed operating range, required operating the motor at higher flux densities than normally used in commercial induction machines. Figure 2 is a finite element model of the induction motor design at the no-load condition. The most saturated region of the machine is operating at a peak flux density value of 2.4 T, which is considerably higher than typically used. Actually, the 2.4 T only occurs at one point in the rotor tooth section and the majority of the saturated regions are limited to 2.0 to 2.2 T, which is within the range of some industrial motor designs.

However, in the 0-200 rpm starting region, much higher values of flux densities had to be employed. In this low-speed region, the flux must be increased substantially to deliver the same torque the motor delivers in the 1,000-6,000 rpm speed range. This higher flux density is achieved at the expense of much higher magnetizing current so the torque/ampere ratio decreases. The final design results are presented in Figure 3.

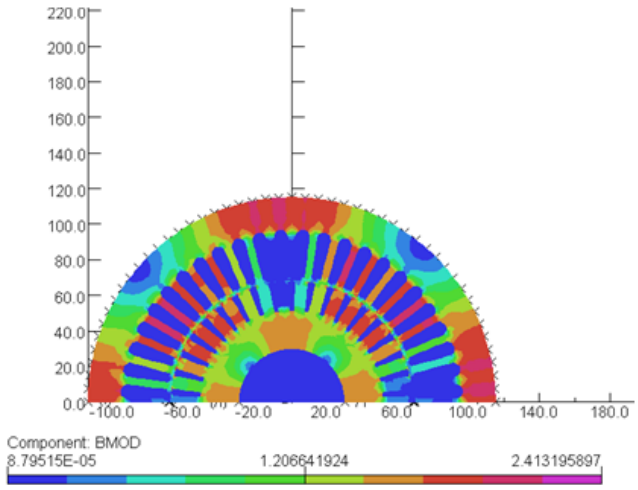

Figure 2. No-load flux density map

In spite of the compact envelope dimensions of the machine and the high levels of magnetic saturation, the baseline design achieved 91.9% efficiency at 50 kW and 91.7% efficiency at 100 kW. Table III itemizes the calculated losses under the nominal (50 kW) and the maximum power (100 kW) loads.

TABLE III. LOSSES AND CALCULATED EFFICIENCY

	Continuous Duty 50 kW	Maximum Power 100 kW
Loss Element	[W]	[W]
Core	1,881	1,751
Stator Copper	956	3,153
Rotor Copper	507	2,315
Stray Load	749	1,499
Friction/Windage	294	287
Total Losses	4,387	9,005
Calculated Efficiency	91.9%	91.7%

Another major design factor was achieving the torque required, particularly in the low speed operating range, i.e. below 3,000 rpm. As noted in Table II, 260 Nm of torque was required in this speed range. This is 270% of the rated torque at 50 kW and 5,000 rpm and must be delivered intermittently for periods of up to 30 s. Figure 3 displays the calculated and specified torque vs. speed as well as current in the 0 to 3,000 rpm speed range.

A relatively low voltage for this size of machine, 200 VAC, was available for powering the motor. Combining this with the size restriction on the inverter resulted in an 800 A maximum

current limit for operating the motor. This, of course, impacted the motor electromagnetic design and the principal impact was, again, in the 0 to 3,000 rpm speed region. A high torque/ampere design was required. The calculated current vs. speed curve is displayed in Figure 3.

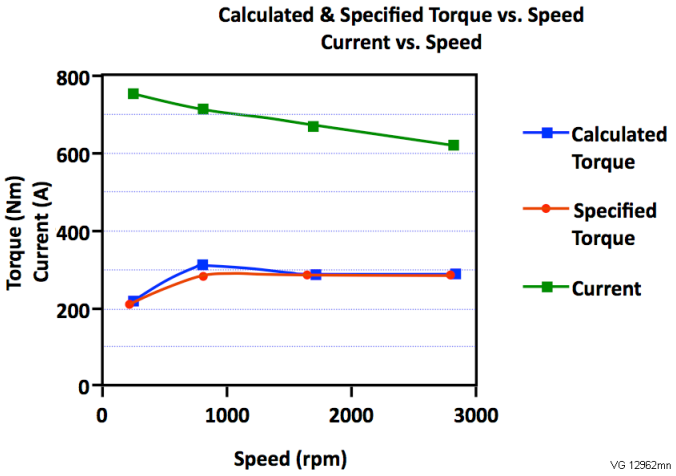

Figure 3. Calculated and specified torque and current vs. speed

In summary, the stringent design requirements created several significant challenges for the electromagnetic design of the PHEV traction motor. The high power density demanded from the restricted envelope dimensions in combination with the need for 270% of rated torque over a wide speed range required the development of a highly magnetically saturated yet efficient electromagnetic design. Further complicating the design was the 800 A current restriction imposed by the constraints on the inverter. Extending design practices from conventional induction motors in the 50 to 100 kW power range would not achieve these goals.

IV. Mechanical Design

Several motor designs were developed and evaluated in an attempt to achieve the required gravimetric power density. The baseline prototype machine design presented in this paper did not achieve the design weight goal of less than 70 kg; however, a production unit using aluminum cast rotor construction was projected to meet this stringent weight limit. Several novel features were incorporated into the design to minimize weight and improve thermal management.

The motor envelope dimensions were dictated by the volume allocations and geometric constraints imposed by vehicle integration considerations. The basic geometry of the motor is shown in Figure 4. The 100 kW motor has an outer diameter of 270 mm (10.625 in.) and a total length from end bell to end bell of 360 mm (14.17 in.) with a total mass of 82 kg.

The stator design is a conventional configuration with several modified features to meet size, mass, and performance requirements. A cross section showing the key features is shown in Figure 5. The M19 laminated stator core is 200 mm (7.87 in.) long with a 48-slot geometry to hold the random wound 4 pole armature winding. The lamination stack is assembled inside the aluminum stator housing with a single keyed interface for torque reaction. The outer aluminum stator housing is actively liquid cooled and provides the primary thermal management for the induction motor; additional detail is presented in the thermal management section of this paper. Lightweight aluminum end bells are designed to house the bearings and shaft seal and provide rigid support for the high speed rotor.

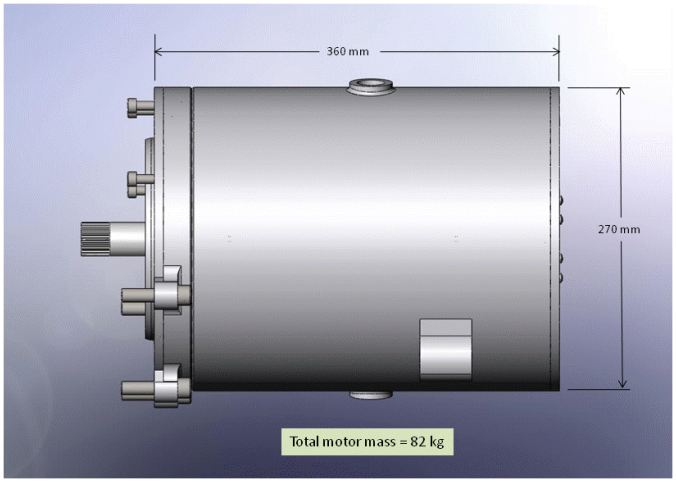

Figure 4. Induction motor envelope dimensions

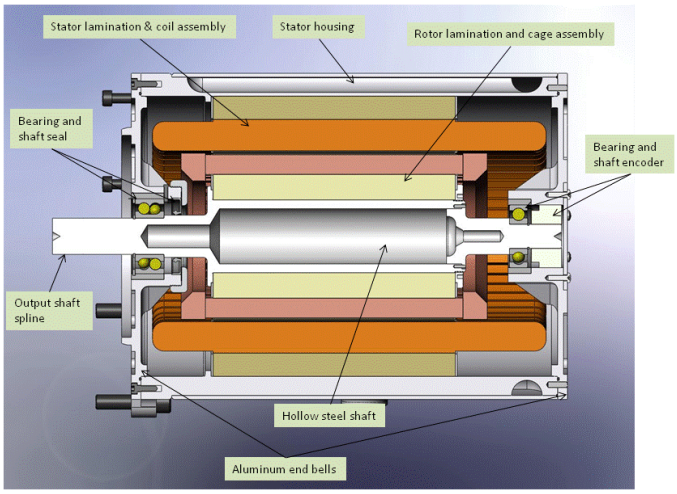

Figure 5. Section view with major components identified

The rotor lamination stack is also 200 mm (7.87 in.) long with a 38-slot geometry. The rotor cage assembly has an outer diameter of 138 mm (5.41 in.) and is a copper bar design with silver braze connections joining the bars to the copper end rings. The lamination stack is assembled onto a non-standard larger diameter, two-piece hollow steel shaft. The hollow shaft design is utilized to enable conventional rotor assembly practices and to mitigate lamination stresses. An additional benefit to the hollow shaft design is that it significantly reduces mass in the motor assembly.

The following sections present some of the design challenges and novel solutions developed for the high performance motor.

A. Stator Housing Cooling Channels

The motor design specification required a totally enclosed, liquid cooled configuration to prevent contamination and ensure adequate life in the harsh under-hood operating environment of the motor. This is achieved with a set of cooling channels in the aluminum motor housing. The cooling channels provide an interesting challenge to trade sufficient cooling performance against stator weight constraints and stiffness which impacts the structural dynamic (vibration) characteristics. The baseline motor design (Fig. 6) has a single coolant inlet on top and in the center of the housing. Upon entering the motor stator housing, the coolant flow then splits in both axial directions down the semicircular coolant passages. The coolant passages then follow an axial serpentine path around the stator housing. The two coolant paths join again at the bottom center of the motor stator housing to form a single coolant outlet. The challenge in this cooling design is to maximize the size of the coolant passages and still maintain adequate bending stiffness in the stator housing to manage rotor dynamics.

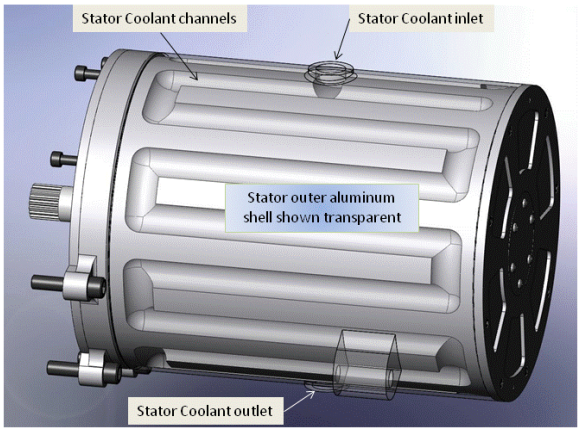

Figure 6. Liquid cooling channels (outer housing removed for clarity)

B. Lightweight End Bells

The end bell design provides a unique challenge for this motor design, both mechanically and thermally. To minimize weight in the motor design, the end bells are constructed of aluminum with a thin web cross section and stiffening gussets to support a cylindrical bearing housing at the center (Fig. 5). The aluminum end bells feature an intermediate steel sleeve to maintain the proper interference fit for the rolling element bearings over the -20°C to 85°C operating temperature range of the motor. The steel sleeves ensure that the radial preload on the outer bearing race stays within acceptable limits even with the high coefficient of thermal expansion of aluminum. The steel sleeve must have a thick enough wall cross section to minimize inward radial deflections as the aluminum end bell shrinks at the low end of the operating temperature range. This steel sleeve must also be installed in the aluminum end bell with sufficient radial interference to insure that it remains fixed as the end bell grows at the upper end of the operating temperature range.

The aluminum end bells are also assumed to provide cooling for the bearings and the rotor and stator winding end turns. The end bells are mechanically attached to the actively cooled stator housing, providing a low resistance path for thermal conduction from the end bells to the housing. Concepts to incorporate active liquid cooling of the end bells were also explored; however, the initial thermal analysis indicated that this is not required.

C. Bearings

High precision rolling element bearings were selected for the high speed motor application. The drive end bearing and shaft seal configuration was specified to facilitate the interface with the vehicle transmission. The bearing is a preloaded duplex pair of 40 mm angular contact ball bearings with a Teflon lip seal to isolate the bearings from the rotor cavity. This bearing pair is designed to manage both radial and thrust loads for the machine. Although the interface to the transmission was not finalized, this bearing configuration potentially allows cooling and lubrication of the drive end bearing using oil flow from the transmission cooling system.

The non-drive end bearing is a 20 mm, single row, sealed ball bearing selected to minimize bearing losses at high speed and reduce the thermal load on the end bell. A sealed bearing with high temperature grease is required because no other lubricant is present on this end of the motor.

D. Hollow Rotor Shaft

Another unique feature of the high speed motor is the hollow shaft design. With a peak design speed of 9,600 rpm, it becomes a design challenge to keep the steel lamination and rotor cage assembly properly preloaded on the steel shaft. Maintaining radial compression between the rotor core and shaft is required for proper torque transmission and to ensure balance retention over the operating speed range. The core interference fit must be designed to manage both spin loading and thermal growth throughout the operating speed and power range of the motor. The design must balance the need for adequate residual preload at full speed and maximum differential temperature against high lamination stresses in the at-rest, cold condition. A 1-D nested ring analysis code was used to evaluate a range of assembly interferences and operating conditions for various shaft and rotor core designs.

A small diameter solid steel shaft will exhibit minimal radial growth due to spin loads, requiring the laminations to be assembled with significant radial interference to offset the spin growth of the rotor core. The high radial stiffness of the solid shaft creates a strong dependence of the stresses on the radial interference, resulting in relatively high stresses in the at-rest, cold condition. For the rigid solid shaft, the design interference is approximately 0.0254 mm (0.001 in.) with a tolerance of plus/minus 0.0127 mm (0.0005 in.) This small interference fit with a very tight tolerance is not practical for conventional commercial induction motor manufacturing processes.

A hollow shaft design addresses the manufacturing issues and also provides additional options for improved rotor cooling. The hollow shaft has a lower radial stiffness and increased radial growth in response to spin loads, reducing the required assembly interference. The increased compliance also reduces the sensitivity of the stresses to the interference and increases the assembly fit tolerances.

V. Cooling Design and Thermal Analysis

The design of the traction motor was specified as a totally enclosed liquid cooled design. The liquid coolant was specified as a 50%-50% water-glycol mixture with a temperature of 65°C at the inlet of the motor. A serpentine stator cooling channel configuration was selected, with cooling channels running axially down the length of the housing. A total channel length of 5.8 m (228 in.) was achieved with this configuration, with two parallel paths of 2.9 m (114 in.) length. The total coolant flow rate of 30 liter per minute (7.93 gpm) was defined by the vehicle cooling system; the coolant flow velocity in the cooling channel is approximately 1 m/s. In this cooling design, the I^2R losses of the armature windings in the core region and the stator core losses are removed by forced liquid cooling in the stator housing. The I^2R losses in the armature winding end-turns are to be removed by end-cavity air flow. To simplify the analysis a two-dimensional (2-D) thermal modeling effort was conducted; the simplified motor model used for the thermal analysis is shown in Figure 7.

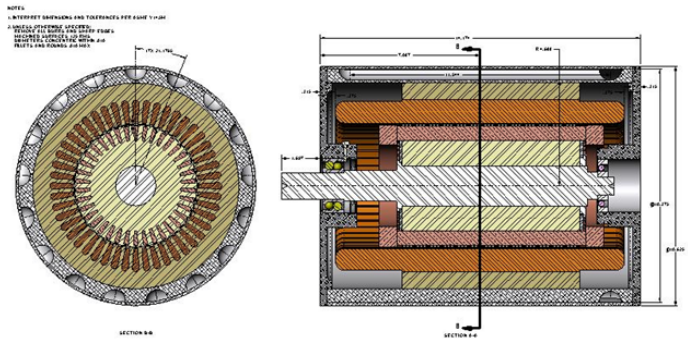

Figure 7. Simplified model used in thermal analysis

For the rotor cooling, I^2R losses of the extended copper bars and copper end rings are removed by the end-cavity air flow. Losses of rotor copper bars in core region and rotor core lamination are assumed to be entirely removed by forced stator liquid cooling through radial heat-transfer paths to the stator core, including vortex-induced convection in rotor/stator air gap [1] and conduction in the stator laminations.

In the 2-D planar finite-element thermal modeling, a 0.076-mm (0.003-in) uniform air gap between rotor conductor bars and surrounding rotor lamination was assumed. Thermal contact resistance at the interface of the stator laminations and stator cooling jacket was also considered. There are 36 copper wires in each stator slot. These 36 conductors in each stator slot were not modeled individually; instead, the copper, wire insulation and potting resin were modeled using equivalent smeared properties in the top and bottom halves of each slot.

The motor has been designed to be operated under various power ratings and rotor speeds. The representative thermal analysis results presented in this paper are those obtained for 50 kW continuous duty operation at 5,000 rpm. Since motor component heat losses are dependent on the component temperatures, after several thermal analysis iterations, a temperature of 280°C was used in the rotor loss calculation and a temperature of 125°C was used in the stator loss calculation. The predicted motor component losses are included in Table IV. In the finite-element thermal modeling, the surface, stray load, and friction and windage losses were assumed to be evenly divided between the rotor and stator.

TABLE IV. Calculated Motor Component Heat Losses Used in Thermal Analysis.

Component	Heat Loss (W)
Rotor Copper Bars	458.7
Rotor Copper End Rings	48.5
Stator Copper Wires	955.8
Stator Core Teeth	493
Stator Core Yoke	747.6
Surface	640.8
Stray Load	749.4
Friction and Windage	294.1
Total Loss	4387.9

Based on the 50 kW continuous duty case, the average and exit stator coolant temperatures were calculated to be 66.2°C and 67.4°C, respectively. The coolant Reynolds number and convection heat transfer coefficient calculated at the average coolant temperature are 15,427 and 3,500 W/(m^2K), respectively. The steady-state motor rotor and stator temperature distributions are shown in Figures 8 and 9.

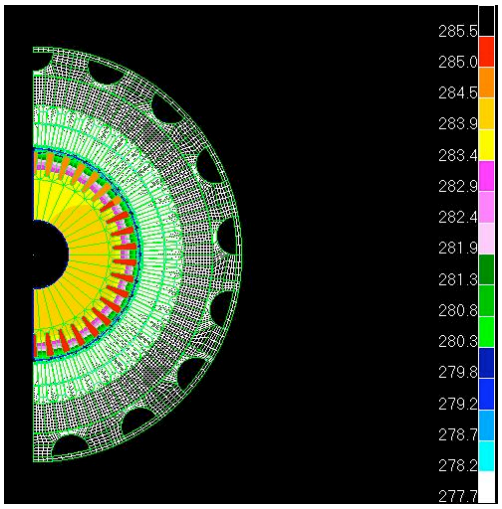

Figure 8. Contour plot of rotor temperatures

The stator is well cooled by the forced liquid cooling with a predicted maximum temperature of only 121.5°C, which is comfortably below the stator insulation temperature limit. The projected maximum rotor temperature is 285.5°C. The rotor temperature prediction presented here is significantly overestimated because the 2-D planar thermal model ignored the axial heat dissipation through the rotor bars and end rings. Forced convection cooling caused by the rotational airflow in the motor end cavities will decrease the maximum rotor temperature presented here. Additional modeling of these effects is needed to confirm acceptable maximum temperatures.

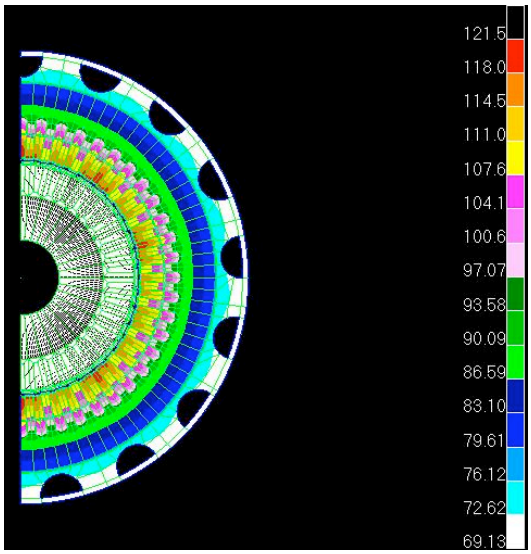

Figure 9. Contour plot of stator temperatures

VI. COMPARISON TO OTHER HYBRID AND ELECTRIC VEHICLE DRIVE MOTORS—BUILD/TEST PROGRAM

The subject of electric motors suitable for integration into hybrid electric or all electric vehicles has attracted significant attention in the last two decades. Several representative publications on this subject are listed in references [2] through [7].

A direct comparison of published data against the motor reported herein is difficult because many of the references do not provide specific dimensional and performance data. This is understandable because of competitive reasons. However, Finken et al. [5] did provide a table comparing the power densities of several different types of motors used in electric vehicle applications. The data in the first four columns of Table V is reproduced from Finken [5]. The last column labeled UT-CEM is the data applying to the motor described in this paper.

TABLE V. COMPARISON OF INDUCTION MOTOR WITH OTHER TYPES OF ELECTRIC VEHICLE MOTORS

	DC	IM	PMSM	SRM	UT-CEM
Power, kW	30	30	30	30	100
Number of pole pairs	5	2	6	12/8	2
Maximum efficiency %	84	89	97	88	92
Volume dm^3	19.2	12.1	4.9	11.8	20.6
Power density kW/dm^3	1.6	2.5	6.1	2.6	4.9

The power density of the UT-CEM induction motor exceeds all of the machines published by Finken except for the permanent magnet synchronous machine (PMSM). As noted by Finken, the PMSM has the disadvantages, compared to induction motors, of limited overload capability due to demagnetization, high cost due to the expensive permanent magnets and the inherent temperature limitation of the permanent magnets.

The performance data reported in this paper, Finken et al. and several of the other references is based on calculated data. An algorithmic software procedure called VICA was used for the design of the UT-CEM machine. VICA has been in use since the 1980's and was used by at least two industrial motor manufacturers so it has a long history of good correlation with test. The final VICA design was also verified with a finite element model.

VII SUMMARY AND CONCLUSIONS

The paper presents the performance requirements and preliminary design of a lightweight 100 kW traction induction motor for a PHEV application. The performance specification includes challenging continuous duty and peak power requirements, along with high torque requirements at the low end of the operating speed range. Motor design was further complicated by the relatively low voltage and current capacity of the battery and traction inverter; the design of these components was dictated by vehicle integration issues. The totally enclosed, liquid cooled motor design features novel coolant channel geometry to minimize the impact of the coolant passages on the structural properties of the aluminum housing. The design also features a hollow shaft designed to mitigate stresses in the laminations and simplify the rotor core assembly. Based on the thermal analysis conducted to date, it appears that liquid cooling will effectively manage the thermal loads.

REFERENCES

[1] C. Gazley, Jr. "Heat-transfer characteristics of the rotational and flow between concentric cylinders," *ASME Transactions*, vol. 80, no 1, pp 79-90, January 1958

[2] C.C Chan, "The state of the art of electric and hybrid vehicles," *Proc. IEEE,* vol. 90, no. 2, pp.247-275, Feb. 2002

[3] C. Shumei, L. Chen, S. Liwei, "Study on efficiency calculation model of induction motors for electric vehicles," IEEE Vehicle Power & Prop. Conf., pp. 1-5, Sept. 3-5, 2008

[4] T. Wang, P. Zheng, Q. Zhang, S. Cheng, "Design characteristics of the induction motor used for hybrid electric vehicle," *IEEE Trans. Magn*., vol. 41, no. 1, Jan. 2005

[5] T. Finken, M. Felden, K. Hameyer, "Comparison and design of different electrical machine types regarding their applicability in hybrid electrical vehicles," Proc. Int'l Conf. on Electr. Machines, 2008

[6] J. Faiz, M. Ghaneei, A. Keyhani, A.B. Proca, "Optimum design of induction motors for electric vehicles," *Electr. Machines & Power Sys*., no. 28, pp. 1177-1194, 2000

[7] Z.Q. Zhu, D. Howe, "Electrical machines and drives for electric, hybrid, and fuel cell vehicles," *Proc. IEEE*, vol. 95, no. 4, pp. 746-765, April 2007.